Pore-Scale Investigation of Micron-Size Polyacrylamide Elastic Microspheres (MPEMs) Transport and Retention in Saturated Porous Media

Chuanjin Yao,*[,†,‡,§] Guanglun Lei,*[,†] Lawrence M. Cathles,[§,‖] and Tammo S. Steenhuis*[,‡]

[†]School of Petroleum Engineering, China University of Petroleum (East China), Qingdao, Shandong 266580, People's Republic of China
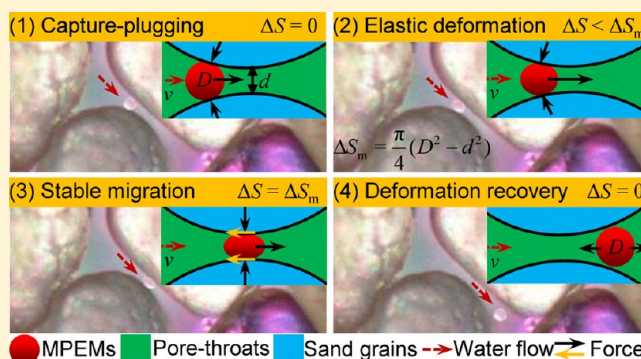
[‡]Department of Biological and Environmental Engineering, Cornell University, Ithaca, New York 14853, United States

[§]KAUST-Cornell Center for Energy and Sustainability, Cornell University, Ithaca, New York 14853, United States

[‖]Department of Earth and Atmospheric Science, Cornell University, Ithaca, New York 14853, United States

S *Supporting Information*

ABSTRACT: Knowledge of micrometer-size polyacrylamide elastic microsphere (MPEM) transport and retention mechanisms in porous media is essential for the application of MPEMs as a smart sweep improvement and profile modification agent in improving oil recovery. A transparent micromodel packed with translucent quartz sand was constructed and used to investigate the pore-scale transport, surface deposition-release, and plugging deposition−remigration mechanisms of MPEMs in porous media. The results indicate that the combination of colloidal and hydrodynamic forces controls the deposition and release of MPEMs on pore-surfaces; the reduction of fluid salinity and the increase of Darcy velocity are beneficial to the MPEM release from pore-surfaces; the hydrodynamic forces also influence the remigration of MPEMs in pore-throats. MPEMs can plug pore-throats through the mechanisms of capture-plugging, superposition-plugging, and bridge-plugging, which produces resistance to water flow; the interception with MPEM particulate filters occurring in the interior of porous media can enhance the plugging effect of MPEMs; while the interception with MPEM particulate filters occurring at the surface of low-permeability layer can prevent the low-permeability layer from being damaged by MPEMs. MPEMs can remigrate in pore-throats depending on their elasticity through four steps of capture-plugging, elastic deformation, steady migration, and deformation recovery.

(1) Capture-plugging $\Delta S = 0$ (2) Elastic deformation $\Delta S < \Delta S_m$

$\Delta S_m = \frac{\pi}{4}(D^2 - d^2)$

(3) Stable migration $\Delta S = \Delta S_m$ (4) Deformation recovery $\Delta S = 0$

● MPEMs ▬ Pore-throats ▬ Sand grains --▶ Water flow ⇒ Force

1. INTRODUCTION

Extracting a greater volume of the oil trapped in rock pores is fundamental to meet future oil demand.[1,2] Oil recovery from a conventional reservoir is characterized by three stages. In primary recovery, the pressure of the reservoir pushes the crude oil to the surface. The secondary recovery relies on pressurized gas and water injection to drive the residual crude oil. Water and gas injection leads to bypass flow due to either an unfavorable mobility ratio between displacing and displaced fluid or heterogeneity in permeability.[3] As a result, a large fraction (up to 70%) of the oil is not contacted by the injected fluid. Tertiary or enhanced oil recovery (EOR) involves removing these remaining hydrocarbons. One of the more promising methods is to block the path through which the injected fluid flows by using micrometer-size polyacrylamide elastic microspheres (MPEMs) and force the flow through section of the reservoir that still contains the hydrocarbons[4−6] (Supporting Information (SI) S1). MPEM treatment is a cost-effective method, as proven by field applications in the Shengli, Jidong, and Dagang Oilfields in China.[7−9]

The transport and retention of MPEMs in porous media is a complex issue. Their elasticity enables them to pass through the pore-throats after a certain deformation under pressure when they are captured by pore-throats.[10] This is in contrast to conventional particles that have difficulty to remigrate once captured by the pore-throats.[11,12] Few studies have focused on the pore-scale transport and retention mechanisms of these particles. Little is known about how these particles are deposited on pore-surfaces, how they block pore-throats, or on their remigration mechanism of the blocked particles.[13]

Most research to investigate the transport and retention of different types of nano- and submicrometer-particles in porous media involved traditional column experiments.[14,15] Although the breakthrough curves and retention profiles from these column experiments can provide valuable insights, they do not

clearly distinguish the ways that hydrodynamic conditions affect particles transport.[15] In two-dimensional transparent etched-glass micromodels, MPEM transport and retention can be visualized, but these models do not accurately reflect the three-dimensional porous media characteristic of actual reservoirs.[16,17] In addition, the size of MPEMs and that of pores and pore-throats in the etched-glass micromodels are of the same order, and finally these models are problematic to reuse due to difficulties in cleaning after MPEM injection.

In this work, a transparent micromodel packed with translucent quartz sand was constructed to avoid the problems of the etched-glass micromodels. A bright-field microscope was used to obtain the pore-scale images of MPEM transport and retention. On the basis of these images, the mechanisms controlling MPEM transport and retention were theoretically analyzed. Thus, the aim of this research was to elucidate the pore-scale transport, surface deposition-release, and plugging deposition−remigration mechanisms of MPEMs.

2. MATERIALS AND METHODS

2.1. Transparent Micromodel. The transparent micromodel with an interior chamber of 8.0 cm length, 1.5 width, and 0.3 cm depth was constructed from clear acrylic sheets. Details for the manufacture procedures are given in SI S2. This micromodel is a three-dimensional model and can reflect the pores and pore-throats distribution of actual reservoirs more accurately than etched-glass micromodels. Besides, this micromodel is convenient to clean and can be packed with sand repeatedly.

2.2. Materials and Reagents. The micron-size polyacrylamide elastic microspheres (MPEMs) used in this study were prepared through the method reported by Yao et al.[18] The MPEM density is ~1.0 g/cm^3. The initial particle size range is 16.5−63.6 μm, and the d_{ave} value is 27.4 μm (see SI Figure S3). The swelling times $(d/d_{ave})_{max}$ of MPEMs is ~1.8 in NaCl solution of 5000 mg/L at 60 °C.[19] The viscosity of 0.1%−0.4% (mass fraction) MPEM suspension is <2.0 mPa·s at 60 °C, and the pH value is ~7.0. The MPEMs are nonflammable, nonexplosive, noncorrosive, and nontoxic to the environment. Translucent quartz sand provided by AGSCO (Hasbrouck Heights, NJ) was selected as the porous media. The sand was further sieved to a size range of 420−500 μm. Detailed chemical properties of the sand are reported in Zhang et al.[20] Prior to use, the sand was acid-washed to remove surface impurities and to minimize chemically attractive microsites on the sand, as described by Zevi et al.[21] The NaCl solution with a salinity of 5000 mg/L was used as the injected brine water.

2.3. Apparatus and Process. The principal components of the experimental apparatus included a micro pump, three piston containers, a capillary, a steel ruler, a transparent micromodel, a jacket heater, a circulating water bath, a sample collector, a vacuum pump, a bubble tower, a computer, a bright field microscope (KH-7700 Hirox-USA, River Edge, NJ), and imaging software in the computer. The experimental process is schematically illustrated in SI Figure S4.

2.4. Methods and Procedures. The translucent quartz sand was packed into the interior chamber of micromodel to a porosity of ~0.39 cm^3/cm^3. Before each experiment, the micromodel was saturated with deionized (DI) water. Then fluids were added in four phases, as illustrated in SI Figure S5. The first three phases are the same for all four experiments and different for phase 4. In phase 1, one pore volume (PV) of brine water with a salinity of 5000 mg/L NaCl was pumped

into the chamber with a Darcy velocity of 0.02 cm/s. For phase 2, 2.5 PV of MPEM suspension of 0.1% by weight in 5000 mg/L NaCl was supplied to the chamber with the same Darcy velocity of 0.02 cm/s. In phase 3, 1.0 PV of brine water with a concentration of 5000 mg/L NaCl was injected at a Darcy velocity of 0.02 cm/s. In phase 4, two PVs were injected in the chamber consisting of either DI water or brine water with a concentration of 5000 mg/L NaCl at two different fluxes as follows: in Exp 1, two PV of DI water was injected at a Darcy velocity of 0.02 cm/s; in Exp 2, two PV of brine water was injected at a 5-fold increase Darcy velocity of 0.10 cm/s; in Exp. 3, two PV of DI water was injected at a Darcy velocity of 0.10 cm/s and finally in Exp. 4, two PV of brine water with a salinity of 5000 mg/L NaCl was injected at a Darcy velocity of 0.02 cm/s. Pore-scale images were collected with the bright field microscope as per Morales et al.[22] throughout the injection process. The injection pressure was measured with a small piezometer filled with water at the model inlet. The effluent MPEMs concentrations were analyzed using a spectrophotometer (Spectronic 501, Milton Roy, Ivyland, PA) at a wavelength of 590 nm. All experiments were conducted at 60 °C. At the end of each experiment, the relative mass of MPEMs recovered in the effluent (MB$_w$, %) was calculated using eq 1.[23]

$$MB_w = \frac{\int_0^{t_f} C(L, t)\, dt}{C_0 \tau} \times 100\% \tag{1}$$

where C_0 is the injected MPEM concentration, L is the porous media length, τ is the MPEM injection duration, $C(L, t)$ is the effluent MPEM concentration, and t_f is the time after the injection started.

3. RESULTS AND DISCUSSION

3.1. MPEM Transport and Retention in Porous Media. During injection of MPEMs in phase 2, the individual MPEMs remained separated and were suspended throughout the liquid between the sand grains (Figure 1a). It can be clearly observed that MPEMs prefer to enter into large pores and pore-throats
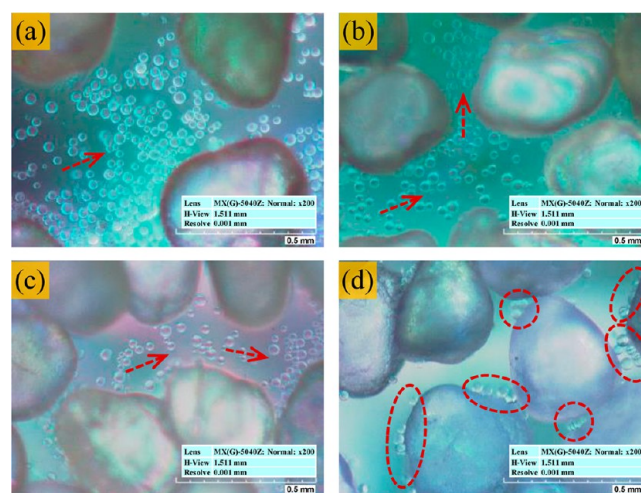

Figure 1. Pore-scale images of MPEM transport and retention in porous media during phase 2 in Exp. 1: (a) suspended and dispersed flow (4 mm from the inlet), (b) preferential flow in large pores and pore-throats (18 mm from the inlet), (c) transport in large pores and pore-throats (36 mm from the inlet), and (d) retention on pore-surfaces and in pore-throats (63 mm from the inlet).

with low flow resistance, and continue to transport within them (Figure 1b,c). In addition, some MPEMs are retained on pore-surfaces or are captured in pore-throats (Figure 1d), due to the surface adsorption, mechanical capture, hydrodynamic effect, and interactions between the MPEMs particles.[24]

Observed breakthrough curves (BTCs) of MPEMs for all four phases and four experiments are shown in Figure 2. In
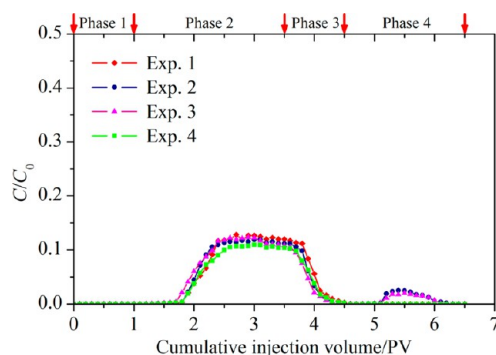
Figure 2. Breakthrough curves (BTCs) of MPEMs throughout the injection process. Phase 1: brine water injection at a Darcy velocity of 0.02 cm/s; phase 2: MPEM suspension injection at a Darcy velocity of 0.02 cm/s; phase 3: brine water injection at a Darcy velocity of 0.02 cm/s; phase 4: (Exp. 1) DI water injection at a Darcy velocity of 0.02 cm/s, (Exp. 2) brine water injection at a Darcy velocity of 0.10 cm/s, (Exp. 3) DI water injection at a Darcy velocity of 0.10 cm/s, and (Exp. 4) brine water injection at a Darcy velocity of 0.02 cm/s.

phase 2, the MPEM suspension was injected and then in phase 3 flushed with an MPEM-free background brine water of same salinity. The MPEMs arrived at the outlet of porous media when the cumulative pore volume was ~1.8 PV which indicated a slight retardation compared to a nonadsorbed solute. At the end of phase 3, only ~10% of the injected MPEMs mass was recovered in the porous media effluent. This result indicates that MPEMs have good resistance to water flushing, and the strength of in-depth plugging is high. In Exp. 1, when the fluid salinity was reduced from 5000 mg/L (Phase 3) to 0 mg/L of DI water (Phase 4), although some MPEMs were released from the pore-surfaces as discussed below, the effluent MPEM concentration was unchanged, as indicated by the BTCs of Exp. 1 in Figure 2. In Exp. 2 and Exp. 3, when the Darcy velocity was increased from 0.02 cm/s (Phase 3) to 0.10 cm/s (Phase 4), some MPEMs were released from the pore-surfaces and remigrate out of the porous media, which performed at the recovery of the effluent MPEM concentrations by ~0.7% in phase 4 as indicated by the BTCs (Exp. 2 and Exp. 3) in Figure 2. While almost no MPEM mass was recovered in the porous media effluent when the velocity was fixed at 0.02 cm/s in phase 4 as indicated by the BTCs (Exp. 4) in Figure 2. The results indicate that the increase of Darcy velocity not only influences the MPEM release on pore-surfaces, but also influences the MPEM remigration in porous media.

During phase 2, when MPEMs were injected in the brine water, the pressure at the inlet increased gradually (Figure 3) indicating that conductivity of the porous media decreased due to the blocking of pore-throats. After changing to MPEM-free background brine water in phase 3, the pressure at the inlet decreased gradually, but stayed at an elevated niveau, indicating that some pore-throats remained blocked. In phase 4, increasing the flux by a factor of 5 in Exp. 2 and Exp. 3 (blue and purple line, Figure 3) increased the inlet pressure suddenly
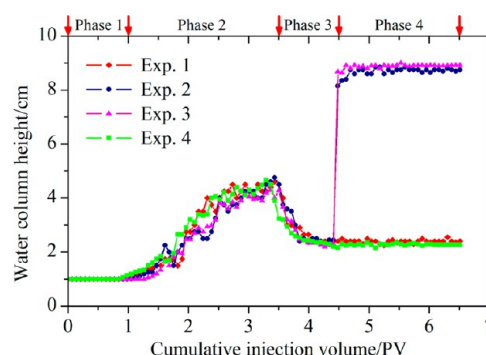

Figure 3. Injection pressure (water column height) change curves throughout the injection process. Phase 1: brine water injection at a Darcy velocity of 0.02 cm/s; phase 2: MPEM suspension injection at a Darcy velocity of 0.02 cm/s; phase 3: brine water injection at a Darcy velocity of 0.02 cm/s; phase 4: (Exp. 1) DI water injection at a Darcy velocity of 0.02 cm/s, (Exp. 2) brine water injection at a Darcy velocity of 0.10 cm/s, (Exp. 3) DI water injection at a Darcy velocity of 0.10 cm/s, (Exp. 4) brine water injection at a Darcy velocity of 0.02 cm/s.

as expected and then stayed steady. In the next sections, we will consider the mechanisms of attachment and release of the MPEMs with grains and the deposition in pore throats.

3.2. MPEMs Deposition and Release on Pore-Surfaces. Whether MPEMs can be deposited on pore-surfaces depends on the properties of the MPEMs and pore-surfaces, and the interactions between the MPEMs and fluid. As reported by Khilar and Fogler,[25] there are four colloidal forces between the MPEMs particles and pore-surfaces, i.e., Vander Waals attraction (F_v), electric double layer repulsion (F_e), Born repulsion (F_b), and acid−base interaction (F_a). In addition, there are five hydrodynamic forces between the MPEMs and fluid, and they are the drag force (F_d), frictional force (F_r), flotage (F_f), gravity (F_g), and inertial force (F_i), respectively. The combined effect of colloidal and hydrodynamic forces controls the transport and deposition states of MPEMs on pore-surfaces (see SI Figure S6). When the resultant force of these nine forces favors adsorption, the MPEMs will be deposited on the pore-surfaces. Observed pore-scale images of MPEMs deposited on pore-surfaces at a salinity of 5000 mg/L NaCl and a Darcy velocity of 0.02 cm/s are shown in Figure 4.
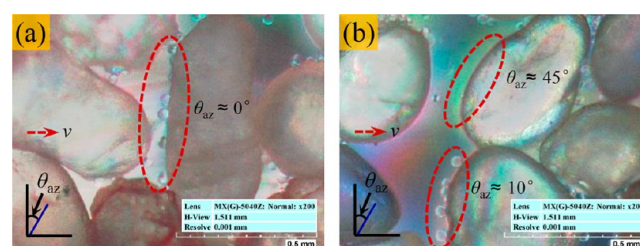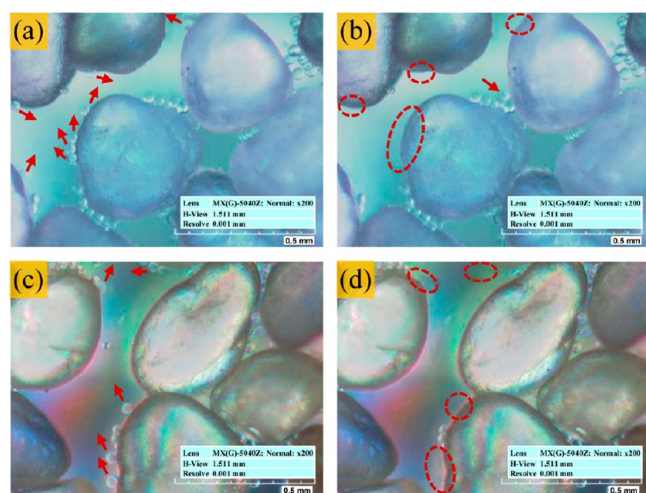

Figure 4. Pore-scale images of MPEMs deposited on pore-surfaces at a salinity of 5000 mg/L NaCl and a Darcy velocity of 0.02 cm/s in phase 3 in Exp. 2: (a) $\theta_{az} \approx 0°$ (upstream stagnation point area, 45 mm from the inlet), (b) $\theta_{az} \approx 10°$ and $\theta_{az} \approx 45°$ (48 mm from the inlet).

It can be seen that the kinetics of this deposition is strongly anisotropic, being more at the upstream stagnation point area and less as the azimuthal angle (θ_{az}) with respect to flow direction increases.

Additionally, when the fluid property and flow state are changed, the deposition state of MPEMs on the pore-surfaces

will be changed too. Whether the MPEMs can be released from the pore-surfaces depends also on the properties of the MPEMs and pore-surfaces, and the interactions between the MPEMs and fluid, i.e., it is controlled by the colloidal and hydrodynamic forces.[25] If the resultant force of colloidal and hydrodynamic forces favors repulsion, then the MPEMs will be released. MPEM release from pore-surfaces is controlled by colloidal and hydrodynamic forces. The colloidal forces largely depend on the content of salt ions in the fluid (i.e., the fluid salinity), while the hydrodynamic forces mainly rely on the fluid velocity.

Figure 5 shows the pore-scale images of MPEM release caused by a change in colloidal and hydrodynamic forces. It is
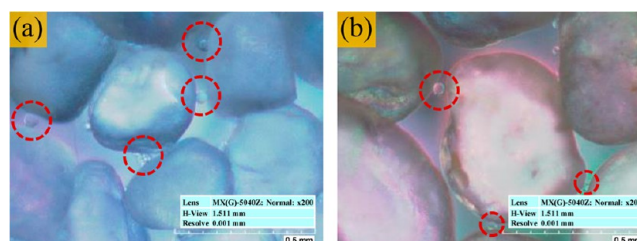

Figure 6. Pore-scale images of MPEMs capture-plugging in pore-throats in phase 3 in Exp. 1: (a) 42 mm from the inlet, and (b) 58 mm from the inlet.

Figure 5. Influence of fluid salinity (C_s) reduction and Darcy velocity (v) increase on MPEMs deposition and release on pore-surfaces: (a) C_s = 5000 mg/L, v = 0.02 cm/s (48 mm from the inlet in phase 3 in Exp. 1); (b) C_s = 0 mg/L, v = 0.02 cm/s (48 mm from the inlet in phase 4 in Exp. 1); (c) C_s = 5000 mg/L, v = 0.02 cm/s (48 mm from the inlet in phase 3 in Exp. 2); and (d) C_s = 5000 mg/L, v = 0.10 cm/s (48 mm from the inlet in phase 4 in Exp. 2).

obvious in Figure 5a,b, that when the fluid salinity is reduced from 5000 mg/L to 0 mg/L in phase 4 or in Figure 5c,d, the Darcy velocity is increased from 0.02 to 0.10 cm/s in phase 4, the MPEMs deposited at the upstream stagnation point area of pore-surfaces will be released. It is obvious that the velocity change mainly affects the drag force. The greater the velocity, the larger the drag force becomes. Thus, some of the MPEMs will be released at greater Darcy velocity. In addition, the MPEM retention is affected by the depth of the secondary minimum. A secondary minimum exists for saline water and holds the MPEMs at the surface.[14] When DI water is added, the secondary minimum disappears, and the MPEMs are released.

3.3. Mechanisms for Plugging Pore-Throats with MPEMs.
The three mechanisms for plugging pore-throats with MPEMs in porous media are capture-, superposition-, and bridge-plugging.

(1) *Capture-Plugging* occurs when an MPEM becomes stuck in a pore-throat with a smaller diameter than the MPEM particle size, as shown in Figure 6. The main forces acting on these MPEMs include the driving force of fluid (F_{df}) and supportive force of pore-throat walls (F_s), as shown in SI Figure S7. Increasing the MPEM particle size, MPEM concentration, and fluid velocity and the smaller elasticity are related to increased plugging.[26,27] This plugging mechanism is similar to the Jamin effect of

bubbles. The similarity lies in the fact that they both can produce an additional flow resistance. The difference is that the Jamin effect relies on the interfacial tension (IFT) of bubbles, while the MPEM capture-plugging phenomenon depends on the elasticity of MPEMs.

(2) *Superposition-Plugging* is different from capture-plugging in that it involves several MPEMs that are larger than the pore-throats. The number of MPEMs can vary from two to four or more, as shown in Figure 7. It is equivalent to
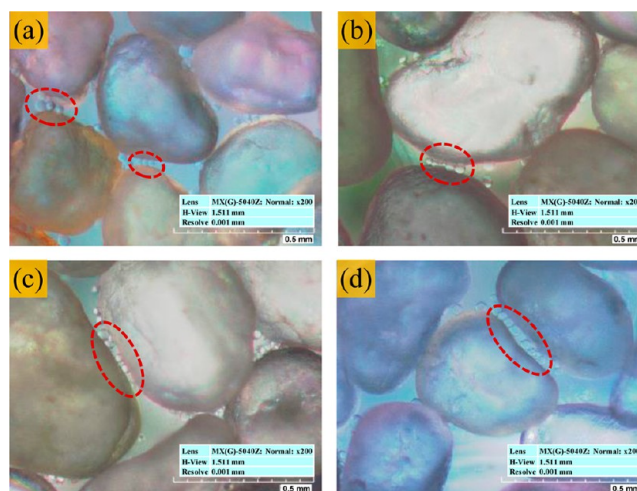

Figure 7. Pore-scale images of MPEM superposition-plugging in pore-throats with MPEM quantities of (a) three (43 mm from the inlet), (b) five (44 mm from the inlet), (c) six (46 mm from the inlet), and (d) seven (49 mm from the inlet) in phase 3 in Exp. 1.

the superposition principle of the Jamin effect. Thus, for the same pore-throat, the superposition-plugging resistance to flow is obviously greater than for capture-plugging. This plugging mechanism is very important to enhance the plugging strength of MPEMs in actual reservoirs.

(3) *Bridge-Plugging* involves plugging by two or more MPEMs that are smaller than pore-throats, as demonstrated in Figure 8. The main forces acting on these MPEMs include the driving force of fluid (F_{df}), supportive force of pore-throats walls (F_s), extruding force (f_e), and frictional force (f_f) between MPEMs. Taking the bridge-plugging of two MPEMs for example, the main forces acting on MPEMs are given in SI Figure S8a. When the relative movement between the two MPEMs is ignored, the two MPEMs can be simplified to an equivalent large MPEM, as shown in SI Figure S8b (where F_{df} is the resultant force of F_{df1} and F_{df2}). The
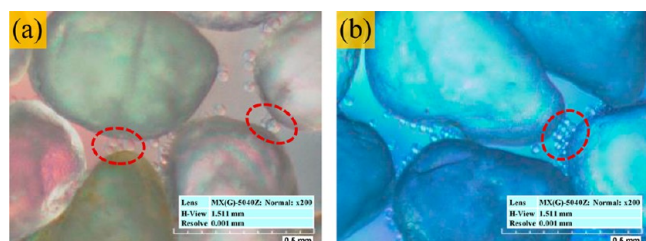
Figure 8. Pore-scale images of MPEM bridge-plugging in pore-throats in phase 3 in Exp. 1: (a) 40 mm from the inlet, and (b) 41 mm from the inlet.

bridge-plugging strength is clearly affected by the pore-throat size, MPEM particle size, MPEM elasticity, MPEM quantity in bridges, and compaction degree of MPEMs. In general, a greater number of MPEMs in a bridge causes more compaction and more resistance to water flow. Bridge-plugging provides an efficient way for MPEMs to plug large pore-throats in actual reservoirs.

3.4. Mechanism for Interception with MPEMs Particulate Filter. MPEM particulate filters occur mainly at the entrance of pore-throats that are filled with MPEMs but not completely closed to flow, as shown in Figure 9. In addition,
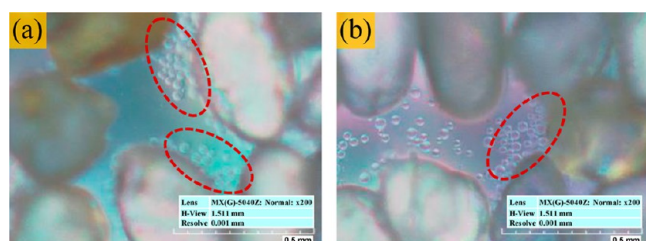
Figure 9. Pore-scale images of MPEM interception with MPEM particulate filters in phase 2 in Exp. 1: (a) 10 mm from the inlet, and (b) 14 mm from the inlet.

this particulate filter forms at the surface of low permeable zones. Interception with MPEMs particulate filter affects the fluid flow in actual reservoirs in two ways. First, it enhances the plugging of pore-throats forcing the influent to follow a different path. Second, it protects the low-permeability zone[18] by intercepting the MPEMs before entering, thus preventing these MPEMS from damaging this zone, as shown in SI Figure S9. The intercepted MPEMs near pore-throats or low-permeability zones are unstable and can be flushed away easily in actual reservoir.[6]

3.5. Mechanisms for Remigration of MPEMs in Pore-Throats. When MPEMs plug pore-throats, there is still a possibility as shown by the decrease in pressure at the inlet in Figure 3, that depending on the elasticity and fluid pressure difference, MPEMs can pass through the pore-throats after capturing. In Figure 10a, an MPEM is captured by a pore-throat. When the pressure difference between both ends of the pore-throats is great enough, the MPEM deforms and gradually enters into the pore-throat (Figure 10b). Further down in the pore-throat, the MPEM transforms to an ellipsoid, and then it continues to migrate in the pore-throats smoothly (Figure 10c). After the MPEM passes through the pore-throat, it will recover to its original shape and size quickly (Figure 10d) as a result of its chemical and physical charaterisics.[17] Additionally, the fluctuant variation of the injection pressure throughout the
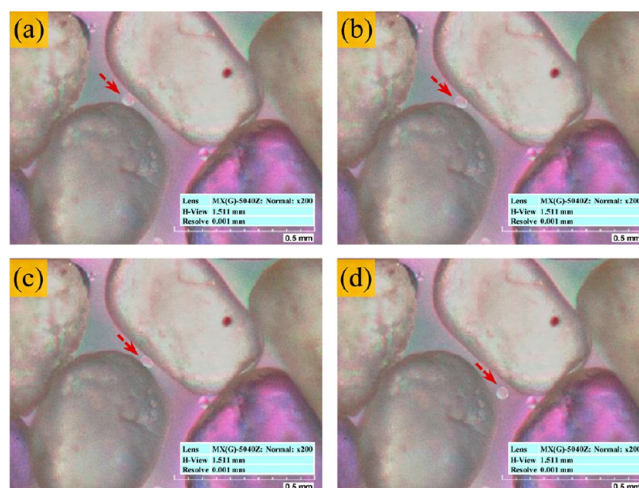
Figure 10. Pore-scale images of MPEMs remigration in pore-throats in phase 4 in Exp. 2 (37 mm from the inlet): (a) capture-plugging, (b) elastic deformation, (c) steady migration, and (d) deformation recovery.

injection process (Figure 3) also indirectly indicates the remigration phenomenon of MPEMs in pore-throats.

Whether the MPEMs can pass through the pore-throats depends on the pressure difference between both ends of the pore-throats, pore-throat size, MPEM particle size, and MPEM deformability. In general, the smaller the pore-throat size, the greater the required pressure difference to push the colloid through the pore-throats. Figure 11 shows the forces acting on MPEMs while they remigrate in pore-throats. Initially, the main forces acting on the MPEMs include the driving force of fluid (F_{df}) and the supportive force of pore-throat walls (F_s) (see Figure 11a). Once the MPEMs are in the pore throats, they deform elastically, and the friction between the walls and the deformed MPEMs need be taken into account in the force balance (see Figure 11b). When the MPEMs enter further into the pore-throats, the deformation of MPEMs reaches the maximum value, and the friction force (F_τ) is the greatest, and the force needed to push MPEMs through the pore-throats reaches a maximum value (ΔP_{max}). Once through the narrowest part of the pore-throats, the MPEMs migrate easily with a decreasing friction force (see Figure 11c). Finally, when the MPEMs leave the pore-throats completely, the MPEMs recover to their original shape and size quickly, and the fluid flow resistance also decreases rapidly (see Figure 11d).

For the MPEMs in this work, the elastic modulus (E) is ∼0.058 kPa, the Poisson's ratio (μ) is ∼0.3, and the friction drag coefficient of pore-throat walls (f) is ∼0.011.[19,28] For the remigration of MPEMs with a diameter of 40 μm in pore-throats with a diameter of 30 μm, it can be calculated using the theory in SI S10, that the maximum additional flow resistance (ΔP_{max}) is ∼0.036 kPa, and the additional flow resistance (ΔP_f) for the stable migration of MPEMs in pore-throats is ∼0.0004 kPa. The results quantitatively indicate the additional flow resistance values of MPEMs remigration in pore-throats.

Additionally, although only the remigration mechanism of single MPEM in pore-throats was observed in the experiments, it can be imaged that the MPEMs occurring superposition-plugging and bridge-plugging in pore-throats are expected to pass through the pore-throats, depending on their elasticity. In these cases, the required pressure difference between the both ends of the pore-throats would be greater.
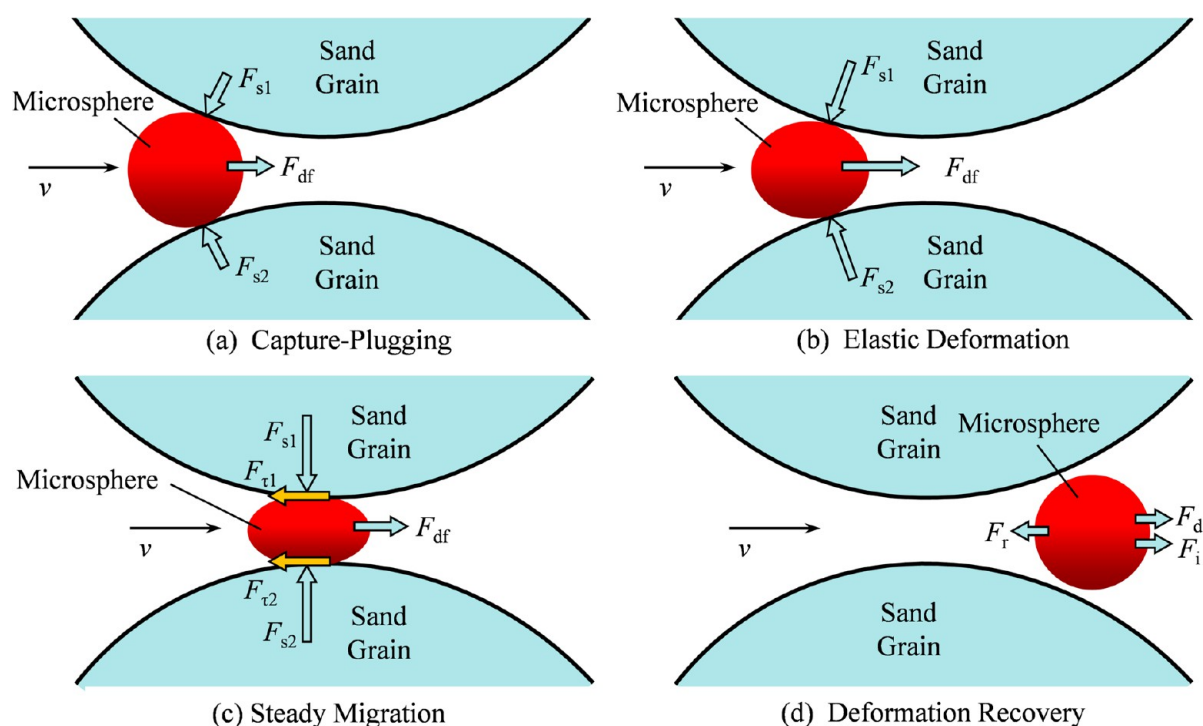
Figure 11. Force analysis for remigration of MPEMs in pore-throats.

■ ASSOCIATED CONTENT

Ⓢ Supporting Information

S1, Principle of MPEMs treatment; S2, manufacture procedures of transparent micromodel; S3, initial particle size distribution of MPEMs in deionized water; S4, experimental setup of MPEMs transport in porous media; S5, experimental flowchart of MPEMs transport in porous media; S6, colloidal and hydrodynamic forces acting on MPEMs; S7, force analysis for capture-plugging pore-throats with MPEMs; S8, force analysis for bridge-plugging pore-throats with MPEMs; S9, interception with MPEMs particulate filter at low-permeability layer surface; and S10, theory for remigration of MPEMs in pore-throats. This material is available free of charge via the Internet at http://pubs.acs.org.

■ AUTHOR INFORMATION

Corresponding Author

*Phone: +1 607 279 8357 (C.Y.); +86 13854637389 (G.L.); +1 607 255 2489(T.S.S.). E-mail: cy375@cornell.edu (C.Y.); leiglun@upc.edu.cn (G.L.); tss1@cornell.edu (T.S.S.).

Notes

The authors declare no competing financial interest.

■ ACKNOWLEDGMENTS

■ REFERENCES

(1) Xiong, C. M.; Tang, X. F. Technologies of water shut-off and profile control: An overview. *Petrol. Explor. Dev.* **2007**, *34* (1), 83−88.

(2) Li, G. H.; Zhang, G. C.; Wang, L. Smart profile control by salt-reversible flocculation of cationic microgels and polyacrylamide. *Energy Fuels* **2013**, *27* (11), 6632−6636.

(3) Zitha, P.; Felder, R.; Zornes, D.; Brown, K.; Mohanty, K. Increasing Hydrocarbon Recovery Factors, 2011. SPE Technology Updates Web site. http://www.spe.org/tech/2011/07/increasing-hydrocarbon-recovery-factors (accessed July 11, 2011).

(4) Zhao, H. Z.; Wu, Z. L.; Zheng, X. Y.; Lin, M. Q.; Li, M. Y. Preparation and performance research of water-soluble crosslinked polymer microspheres. *Fine Chem.* **2005**, *22* (1), 62−64.

(5) Sun, H. Q.; Wang, T.; Xiao, J. H.; Chen, H. Novel technique of in-depth profile control step by step by polymer microspheres. *Petrol. Geol. Recovery Eff.* **2006**, *13* (4), 77−79.

(6) Lei, G. L. *New Deep Profile Control and Flooding Technology Using Pore-Scale Elastic Microspheres*; China University of Petroleum Press: Dongying, China, 2011.

(7) Lei, G. L.; Zheng, J. P. Composing of pore-scale polymer microsphere and its application in improve oil recovery. *J. Chin. Univ. Petrol.* **2007**, *31* (1), 87−90.

(8) Yao, C. J.; Lei, G. L.; Gao, X. M.; Li, L. Study on indepth profile control and flooding of pore-scale elastic microspheres under heterogeneous condition. *Pet. Geol. Recovery Eff.* **2012**, *19* (5), 61−64.

(9) Yao, C. J.; Lei, G. L.; Li, W. Z.; Li, L.; Gao, X. M. An experiment and simulation of elastic microspheres enhanced oil recovery (EMEOR). *Energy Sour. Part A-Recovery Util. Environ. Eff.* **2012**, *34* (8), 692−701.

(10) Wang, J.; Liu, H. Q.; Wang, Z. L.; Hou, P. C. Experimental investigation on the filtering flow law of pre-gelled particle in porous media. *Transp. Porous. Med.* **2012**, *94* (1), 69−86.

(11) Jiang, J. F.; Hu, E. A.; Zhao, Q.; Lin, Y. X. Research and application of the water shut-off technique in thin intercalation. *Oil Drill. Prod. Technol.* **2001**, *23* (1), 54−56.

(12) Lun, Z. M. Study on the blockage characteristics of reservoir pores due to suspension particles of injection water. *J. Logist. Eng. Univ.* **2006**, *3*, 30−32.

(13) Venetsianov, E. V.; Rubinstein, R. N. *Dynamics of Sorption from Liquids*; Nauka: Moscow, Russia, 1983.

(14) Sang, W. J.; Morales, V. L.; Zhang, W.; Stoof, C. R.; Gao, B.; Schatz, A. L.; Zhang, Y. L.; Steenhuis, T. S. Quantification of colloid

retention and release by straining and energy minima in variably saturated porous media. *Environ. Sci. Technol.* **2013**, *47* (18), 8256−8264.

(15) May, R.; Akbariyeh, S.; Li, Y. S. Pore-scale investigation of nanoparticle transport in saturated porous media using laser scanning cytometry. *Environ. Sci. Technol.* **2012**, *46* (18), 9980−9986.

(16) Zhang, C. Y.; Oostrom, M.; Wietsma, T. W.; Grate, J. W.; Warner, M. G. Liquid CO_2 displacement of water in a dual-permeability pore network micromodel. *Environ. Sci. Technol.* **2011**, *45* (7), 7581−7588.

(17) Dong, M.; Liu, Q.; Li, A. Displacement mechanisms of enhanced heavy oil recovery by alkaline flooding in a micromodel. *Particuology* **2012**, *10* (3), 298−305.

(18) Yao, C. J.; Lei, G. L.; Gao, X. M.; Li, L. Controllable preparation, rheology and plugging property of micron-grade polyacrylamide microspheres as a novel profile control and flooding agent. *J. Appl. Polym. Sci.* **2013**, *130* (2), 1124−1130.

(19) Yao, C. J.; Lei, G. L.; Li, L.; Gao, X. M. Selectivity of pore-scale elastic microspheres as a novel profile control and oil displacement agent. *Energy Fuels* **2012**, *26* (8), 5092−5101.

(20) Zhang, W.; Morales, V. L.; Cakmak, M. E.; Salvucci, A. E.; Geohring, L. D.; Hay, A. G.; Parlange, J. Y.; Steenhuis, T. S. Colloid transport and retention in unsaturated porous media: Effect of colloid input concentration. *Environ. Sci. Technol.* **2010**, *44* (13), 4965−4972.

(21) Zevi, Y.; Dathe, A.; McCarthy, J. F.; Richards, B. K.; Steenhuis, T. S. Distribution of colloid particles onto interfaces in partially saturated sand. *Environ. Sci. Technol.* **2005**, *39* (18), 7055−7064.

(22) Morales, V. L.; Gao, B.; Steenhuis, T. S. Grain surface-roughness effects on colloidal retention in the vadose zone. *Vadose Zone J.* **2009**, *8* (1), 11−20.

(23) Vitorge, E.; Szenknect, S.; Martins, J. M. F.; Gaudet, J. P. Size- and concentration-dependent deposition of fluorescent silica colloids in saturated sand columns: Transport experiments and modeling. *Environ. Sci.: Process. Impacts* **2013**, *15* (8), 1590−1600.

(24) Bradford, S. A.; Torkzaban, S. Colloid transport and retention in unsaturated porous media: A review of interface-, collector-, and pore-scale processes and models. *Vadose Zone J.* **2008**, *7* (2), 667−681.

(25) Khilar, K. C.; Fogler, H. S. *Migration of Fines in Porous Media*; Kluwer Academic Publishers: Dordrecht, The Netherlands, 1998.

(26) Chauveteau, G. A.; Nabzar, L.; Coste, J. P. Physics and modeling of permeability damage induced by particle deposition. *Proceedings of SPE International Symposium on Formation Damage Control, Lafayette, LA, February 18−19, 1998*; Society of Petroleum Engineers: Richardson, TX, 1998; SPE 39463.

(27) Veerapen, J. P.; Nicot, B.; Chauveteau, G. A. In-depth permeability damage by particle deposition at high flow rates. *Proceedings of SPE European Formation Damage Conference, Hague, The Netherlands, May 21−22, 2001*; Society of Petroleum Engineers: Richardson, TX, 2001; SPE 68962.

(28) Ma, H. W.; Liu, Y. Z.; Li, Y. K.; Tang, X. F.; Qin, H.; Xiong, C. M. Research on flexible particle migration in porous media. *Oil Drill. Prod. Technol.* **2007**, *29* (4), 80−82.